SCIENCE CHINA
Earth Sciences

•ARTICLE•

January 2024 Vol.67 No.1: 222–233
https://doi.org/10.1007/s11430-023-1172-9

The influence of silica on reaction rates and molecular hydrogen (H_2) generation during olivine hydrothermal alteration

Ruifang HUANG[1,2*], Weidong SUN[3], Xing DING[4], Yusheng ZHAO[1], Yibing LI[5] & Xiuqi SHANG[2]

[1] *CAS Key Laboratory of Ocean and Marginal Sea Geology, South China Sea Institute of Oceanology, Chinese Academy of Sciences, Guangzhou 510301, China;*
[2] *SUSTech Academy for Advanced Interdisciplinary Studies, Southern University of Science and Technology, Shenzhen 518055, China;*
[3] *Center of Deep Sea Research, Institute of Oceanology, Chinese Academy of Sciences, Qingdao 266071, China;*
[4] *State Key Laboratory of Isotope Geochemistry, Guangzhou Institute of Geochemistry, Chinese Academy of Sciences, Guangzhou 510640, China;*
[5] *Institue of Geology, Chinese Academy of Geological Sciences, Beijing 100037, China*

Received February 19, 2023; revised August 7, 2023; accepted August 22, 2023; published online December 15, 2023

Abstract Hydrothermal alteration of olivine greatly influences geodynamics and the recycling of volatiles (such as water and carbon) in subduction zones. Silica is an important component of geological fluids, and its influence on the hydrothermal alteration of olivine remains poorly constrained. In this study, we performed experiments at 300–515°C and 3.0 kbar (1 bar=10^5 Pa) by reacting well homogenized mixtures of olivine and silica powders with saline solutions (0.5 mol L^{-1} NaCl). Silica greatly influences the reaction pathways, reaction rates, and molecular hydrogen (H_2) formation during olivine hydrothermal alteration. In experiments at 300°C and 3.0 kbar with mixtures of olivine and 10 wt% silica, olivine was replaced by serpentine and talc. The proportions of serpentine and talc were determined according to standard curves based on infrared spectroscopy analyses. Around 6.5% serpentine and 12% talc were produced after an experimental duration of 7 days, which had no change after a longer period (14 days). Compared to the kinetics in silica-free systems, the rates of olivine hydrothermal alteration in experiments with 10 wt% silica are much lower. The overall reaction is: 4.5Forsterite+5.5$SiO_{2,aq}$+4H_2O=Serpentine+2Talc. With the addition of more silica (20 wt% and 40 wt%), olivine was transformed into talc. The rates of reaction were much faster, e.g., for experiments with olivine and 20 wt% silica, 43% of talc was produced after 14 days, which increased to 77% for experiments with 40 wt% silica over the same period. The overall reaction is: 3Forsterite+5$SiO_{2,aq}$+2H_2O=2Talc. In experiments at 400–505°C and 3.0 kbar, the promoting effect of silica on olivine hydrothermal alteration was also observed, which is closely associated with a decrease in Gibbs free energies of olivine hydrothermal alteration. At 300°C and 3.0 kbar, silica decreased H_2 formed during olivine hydrothermal alteration by around an order of magnitude, resulting in an increase in oxygen fugacity. Based on measured H_2, we calibrated oxygen fugacities, ranging from 0.96 to 3.41 log units below FMQ (fayalite-magnetite-quartz buffer assemblage). This study suggests that the infiltration of SiO_2-bearing fluids into peridotites greatly influences redox conditions and the rates of olivine hydrothermal alteration.

Keywords Olivine hydrothermal alteration, Silica, Serpentinization, Hydrogen, Serpentine

Citation: Huang R, Sun W, Ding X, Zhao Y, Li Y, Shang X. 2024. The influence of silica on reaction rates and molecular hydrogen (H_2) generation during olivine hydrothermal alteration. Science China Earth Sciences, 67(1): 222–233, https://doi.org/10.1007/s11430-023-1172-9

* Corresponding author (email: huangrf@sustech.edu.cn; ruifanghuang_geo@163.com)

1. Introduction

The hydrothermal alteration of olivine has attracted the attention of geologists, biologists, and chemists (e.g., Kelley et al., 2001; Charlou et al., 1998, 2002; Schrenk et al., 2004, 2013; Brazelton et al., 2006, 2012; Lang et al., 2010; Evans et al., 2013). It significantly influences the physical and chemical properties of the oceanic lithosphere (e.g., Escartín et al., 1997, 2001; Scambelluri, 2001; Scambelluri et al., 2004; Guillot and Hattori, 2013), and it also affects microbial habitability at hydrothermal vent fields (e.g., Brazelton et al., 2006, 2012; Schrenk et al., 2013). Hydrothermal alteration greatly decreases the strength, density and seismic velocity of olivine (e.g., Escartín et al., 1997, 2001; Mével, 2003), possibly resulting in an increase in volume (Malvoisin et al., 2020). The hydrothermal alteration of olivine produces serpentine, talc, and chlorite that have abundant H_2O contents. As suggested by experimental studies, serpentine and talc remain stable at depths even greater than 150 km (Ulmer and Trommsdorff, 1995). This suggests that the hydrothermal alteration of olivine may play a significant role for the recycling of H_2O in the subduction zones. In addition, the hydrothermal alteration of olivine produces molecular hydrogen (H_2) that may influence microbial habitability at hydrothermal vent fields (e.g., Kelley et al., 2001; Schrenk et al., 2004; Lang et al., 2010).

Previous experiments on the hydrothermal alteration of olivine were performed mostly with olivine and pure H_2O or saline solutions as starting reactants (Berndt et al., 1996; Allen and Seyfried, 2003; Marcaillou et al., 2011; Okamoto et al., 2011; Malvoisin et al., 2012; McCollom et al., 2016, 2020). Olivine in natural geological settings is commonly associated with silica-bearing minerals such as plagioclase, pyroxene and microcrystalline silica (Hodgkinson et al., 2015). Thermodynamic calculations suggest that silica activity greatly influences the stable mineral assemblages during olivine hydrothermal alteration (Figure 1). Previous experiments about the effect of silica during olivine hydrothermal alteration have been performed with largely scattered silica activity in one sample by up to four orders of magnitude, where a quartz layer (10 mm in length) was in contact with an olivine layer (35 mm in length) (e.g., Oyanagi et al., 2015, 2020). The influence of silica on the rates of olivine hydrothermal alteration remains unclear, e.g., in saline solutions (0.5 mol L^{-1} NaCl), intermediate silica activity is associated with the highest rates of reaction (Oyanagi et al., 2020); in strongly alkaline solutions, the highest silica activity is coupled with the fastest rates of reaction (e.g., Oyanagi et al., 2015). Hydrogen formation in the experiments of Oyanagi et al. (2015, 2020) was not measured. Silica activity also influences H_2 formation during olivine hydrothermal alteration (Frost and Beard, 2007; Beard et al., 2009; Katayama et al., 2010; Seyfried et al., 2011; Miyoshi et al., 2014; Oyanagi et al., 2015; Syverson et al., 2017). However, the coupling between the rates of olivine hydrothermal alteration and H_2 formation in silica-bearing systems remains poorly constrained.

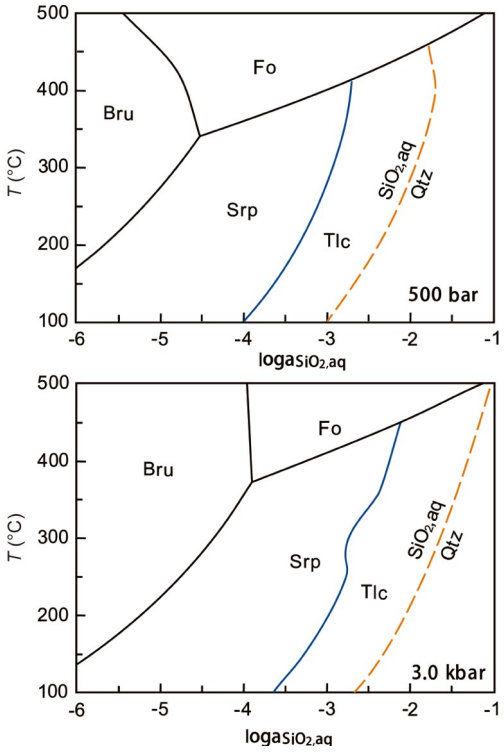

Figure 1 Phase diagrams in the MgO-SiO_2-H_2O system as a function of silica activity calibrated by using SUPCRT92 (Johnson et al., 1992). (a) 500 bar, and (b) 3.0 kbar. Fo, forsterite; Srp, serpentine; Bru, brucite; Tlc, talc; Qtz, quartz. 1 bar=10^5 Pa.

In this study, we conducted hydrothermal experiments at 300–515°C and 3.0 kbar, and well-mixed olivine and silica powders (10–40 wt%) were reacted with saline solutions (0.5 mol L^{-1} NaCl). Compared to previous experiments (Oyanagi et al., 2015, 2020), the thickness of the starting reactants in the experiments of this study is much smaller (<2 mm in length), with a very low silica gradient in one sample. The targets are to (1) study the effect of silica on the pathways, the rates of reaction, and H_2 formation during olivine hydrothermal alteration, and (2) investigate temperature dependence for the influence of silica on olivine hydrothermal alteration.

2. Starting materials and experimental methods

2.1 Starting materials

Olivine grains (Fo=90) were carefully chosen from crushed peridotite (<60 mesh) under a binocular microscope, and those with the inclusion of other mineral phases were discarded. The peridotite occurs as xenoliths in alkaline basalts at Panshishan (Jiangsu province, China) (e.g., Chen et al.,

1994; Sun et al., 1998; Xu et al., 2008).

Olivine grains were cleaned ultrasonically in pure water to remove pyroxene powders adhered to the surface of olivine during peridotite crushing. After that, olivine grains were ground in an agate mortar, and then they were sieved to obtain grain sizes of <30 μm.

Olivine powder and analytical reagent quartz powders were well homogenized in an agate mortar. The total mass of solid reactants is ~50 mg. The solid reactants and saline solutions (0.5 mol L^{-1} NaCl, ~50 mg) were filled into gold capsules (3.6 mm inner diameter, 4.0 mm outer diameter, and 30 mm length). The thickness of the starting reactant is less than 2 mm. Gold capsules have been used as reactors (e.g., Berndt et al., 1996; Malvoisin et al., 2012; Huang et al., 2015, 2016), because gold is not chemically active and does not form Au-Fe alloys under the experimental conditions. Gold capsules were sealed at both ends by using a high-frequency tungsten inert gas welder (PUK3). Then, sealed gold capsules were placed in a drying furnace (100°C) for around half an hour to check leakage, and those with mass differences less than 0.5% were used in hydrothermal experiments.

2.2 Hydrothermal experiments

All experiments were carried out at 300–515°C and 3.0 kbar in cold-seal hydrothermal vessels at Guangzhou Institute of Geochemistry, Chinese Academy of Sciences (Table 1). The capsule, followed with a filler rod (around 6 cm long), was put into a vertically-placed cold-seal vessel. Pressures were achieved by pumping water from a reservoir into the vessel, and they were measured by a pressure gauge with a precision of ±100 bar. Temperatures were monitored with an external K-type thermocouple that was inserted into a hole near the end of the vessel with an accuracy of ±2°C. When finished, the vessels were immersed in ice water, and the temperature of the capsule decreased to <100°C within a few seconds.

2.3 Analytical methods

The amounts of molecular hydrogen (H_2) in gold capsules were determined with an Agilent 7890A gas chromatograph at the State Key Laboratory of Organic Geochemistry, Guangzhou Institute of Geochemistry, Chinese Academy of Sciences. The gold capsule was put in a vacuum glass piercer that is connected to a Toepler pump. The whole device was evacuated to a pressure below 1×10^{-2} Pa, and then the capsule was sliced to release all the gases. The Agilent 7890A gas chromatograph was fitted with a HayeSep Q column (27 m×0.32 mm i.d.), and nitrogen was taken as the carrier gas at a flow rate of 25 mL min^{-1}. The oven temperature was programmed at 60°C for 3 min, raised from 60°C to 180°C at 25°C/min, and kept at 180°C for 3 min. The gas components were calibrated by using an external standard with an accuracy of less than 0.5%. More procedures have been detailed in previous work (Xiong et al., 2001; Pan et al., 2006).

The surface morphology of solid products was characterized by secondary electron using Zeiss Ultra 55 field emission gun scanning electron microscope (SEM) at the Second Institute of Oceanography, State Oceanic Administration of China. An accelerating voltage of 5 kV was used. X-ray diffraction (XRD) patterns were collected using Cu-Kα radiation, 45 kV voltage and 200 mA current on a Rigaku

Table 1 Summary of experimental results[a)]

Sample number	Temperature (°C)	Pressure (kbar)	Starting reactants		W/R ratios	Time (days)	Amounts of minerals in run products (%)			H_2 (mmol kg^{-1})
			Reactant	SiO_2 (wt%)			Tlc	Srp	Ol	
HR106	300	3.0	Ol	0	0.90	10	–	62 (0.1)	38 (0.1)	94
HR76	300	3.0	Ol	0	1.04	27	–	76 (1.7)	24 (1.7)	80
HR119	300	3.1	Ol+SiO_2	10	0.97	7	10 (1.2)	5.5 (0.3)	84.5 (1.5)	37
HR116	300	3.1	Ol+SiO_2	10	0.95	14	12 (3.0)	6 (3.5)	79 (1.3)	8.6
HR112	300	3.1	Ol+SiO_2	20	0.84	14	43 (2.0)	–	57 (2.6)	3.7
HR114	300	3.1	Ol+SiO_2	20	0.84	20	43 (1.4)	–	57 (1.9)	8.5
HR113	300	3.1	Ol+SiO_2	40	0.72	14	77 (1.2)	–	23 (0.4)	3.7
HR115	300	3.1	Ol+SiO_2	40	0.74	20	100 (0.1)	–	0	2.2
HR130	400	3.8	Ol+SiO_2	40	0.90	8	–	–	–	7.1
HR101	505	3.2	Ol+SiO_2	50	0.71	9	100 (0.1)	–	0	3.3
HR103	505	3.0	Ol+SiO_2	50	0.80	14	100 (0.1)	–	0	1.2
HR57*	400	3.0	Ol	0	1.3	19	–	0.5	–	2.0
Fe46**	515	3.6	Ol	0	1.5	17	–	0.5	–	2.2

a) W/R ratios: Water/rock ratios, mass ratios of starting fluids to solid reactants before experiments; Tlc: talc, Srp: serpentine, Ol: olivine; * Olivine with initial grain sizes of 42–59 μm (Huang et al., 2020); ** Olivine with initial grain sizes of 100–177 μm (Huang et al., 2020)

Smartlab X-ray diffractometer at the Southern University of Science and Technology, Shenzhen, China. X-ray data were acquired in a 2θ range of 5°–70° with a step size of 0.01° and a counting time of 10 s per step. Fourier transform infrared (FTIR) spectroscopy analyses were performed with a Bruker Vector 33 FTIR spectrometer at Analytical and Testing Center of South China University of Technology. KBr pellets were made by mixing around 1 mg of sample with 200 mg of KBr. Infrared spectra were obtained at wavenumbers ranging from 400 cm^{-1} to 4000 cm^{-1} at 4 cm^{-1} resolution, and 32 scans were accumulated for each spectrum.

3. Results

3.1 Characterization of minerals in the run products

The XRD patterns of typical run products are illustrated in Figure 2, and infrared spectra and scanning electron microscope images are shown in Figures 3 and 4. In olivine-only experiments at 300°C and 3.0 kbar without silica, olivine was replaced by serpentine (Figure 2). Infrared spectra of the run products show typical modes at 954, 1025 and 1075 cm^{-1} for the stretching vibration of the Si-O group (Figure 3a), indicating the formation of chrysotile (e.g., Foresti et al., 2003; Lafay et al., 2014). Brucite was not formed, possibly due to the dissolution of brucite in saline solutions (e.g., Jöns et al., 2017). In addition, magnetite was not identified using XRD (Figure 2).

For experiments at 300°C and 3.0 kbar with well-homogenized mixtures of olivine and 10 wt% silica powders, olivine was transformed into serpentine and talc. X-ray diffraction peaks of serpentine and talc are very broad (Figure 2), which suggests poor crystallinity. Infrared peaks of run products at 670 and 3677 cm^{-1} also indicate talc formation, and these peaks are ascribed to the stretching vibration of Si-O-Mg and –OH bands, respectively (Liu et al., 2014). Infrared peaks at 954 and 3692 cm^{-1} indicate serpentine formation, which are attributed to the stretching vibration of Si-O and –OH bands in serpentine, respectively (e.g., Foresti et al., 2003; Lafay et al., 2014). Scanning electron microscopy (SEM) images show a fibrous morphology of serpentine (Figure 4), indicating serpentine polymorph is chrysotile (Lafay et al., 2012). In experiments with well-homogenized mixtures of olivine and 20 wt% and 40 wt% silica powders, olivine was transformed into talc without forming serpentine (Figure 2). Infrared spectra of run products show typical infrared peaks of talc at 671 and 3677 cm^{-1} (Figure 3). Infrared peaks for serpentine, however, are lacking (Figure 3). Relic olivine was observed in most experiments at 300°C and 3.0 kbar, which has typical infrared peaks at 503, 606, and 885 cm^{-1} (e.g., Jeanloz, 1980).

In olivine-only experiments at 400–515°C and 3.0 kbar without silica, olivine was almost completely unaltered after

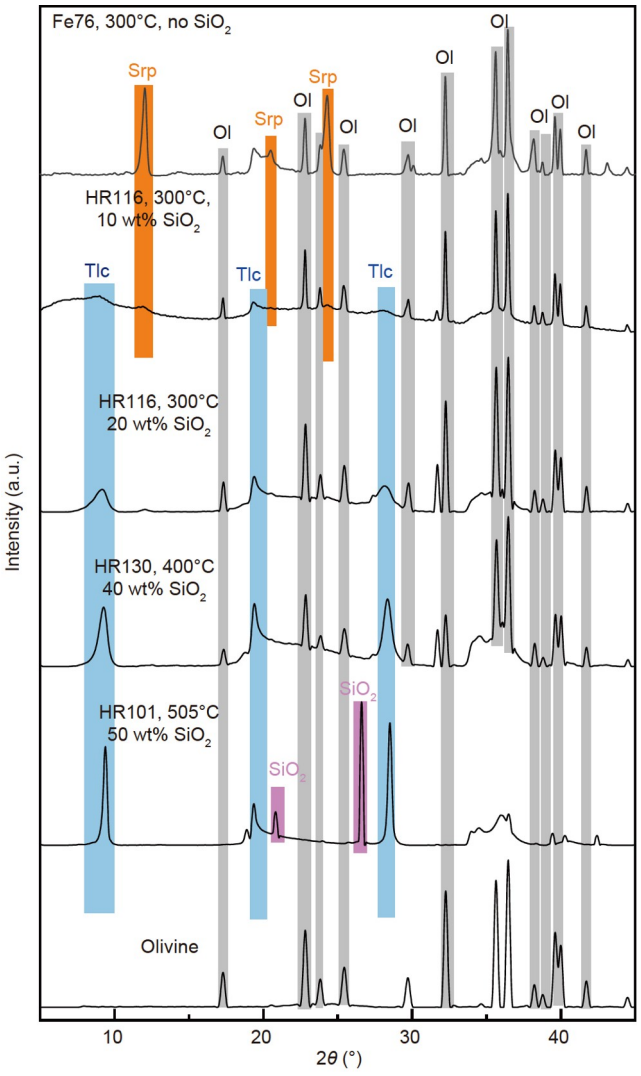

Figure 2 X-ray diffraction patterns of starting olivine and typical solid experimental products. Tlc, talc; Ol, olivine; Srp, serpentine.

17–19 days (Huang et al., 2020). Consistently, previous studies also show that olivine remains stable at temperatures of ⩾350°C (Allen and Seyfried, 2003; McCollom and Bach, 2009). With the addition of silica, intensities of the diffraction peaks for olivine decreased significantly, and intensities of the diffraction peaks for talc increased greatly (Figure 2), indicating that olivine was more extensively hydrothermally altered in the presence of silica. In particular, olivine was completely replaced by talc in experiments at 505°C and 3.0 kbar with the addition of 50 wt% silica powders. The presence of relic silica in the experimental products indicates that silica-saturated conditions have been reached (Figure 2). XRD patterns show that talc has much sharper diffraction peaks at higher temperatures (Figure 2), indicating that talc has better crystallinity with increasing temperatures. SEM images show that talc formed at 505°C and 3.0 kbar had larger grain sizes (~5 μm) than that produced at lower temperatures (~1 μm of grain sizes at 300°C and 3.0 kbar) (Figure 4).

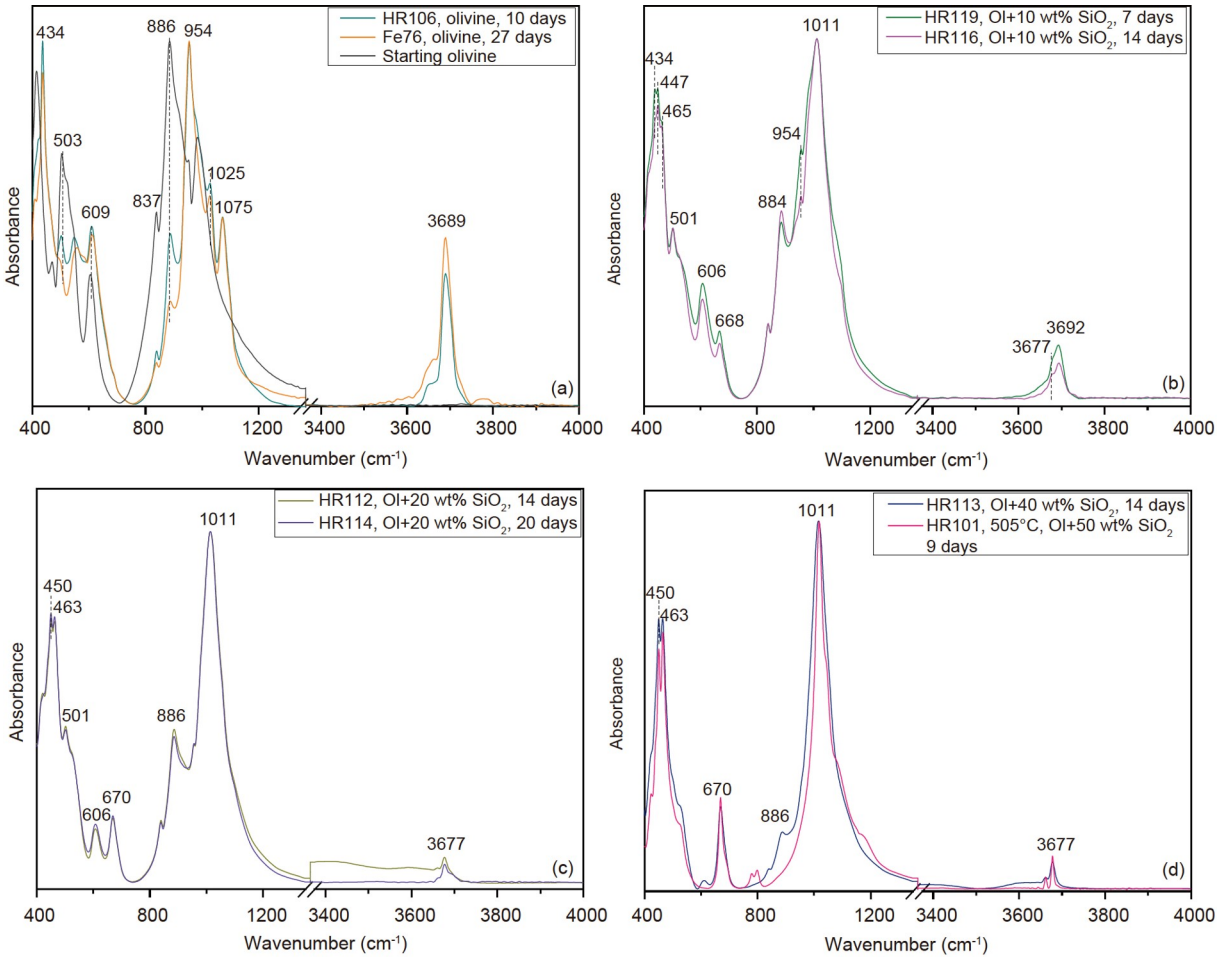

Figure 3 Infrared spectra of starting olivine and solid experimental products. (a) Olivine has typical infrared peaks at 503 and 885 cm^{-1} (Jeanloz, 1980). The intensity of these peaks decreased greatly during olivine hydrothermal alteration, leading to serpentine formation with typical infrared peaks at 954 and 3689 cm^{-1} (Foresti et al., 2003). (b) Experiments at 300°C and 3.0 kbar with well-mixed olivine and 10 wt% silica. Serpentine and talc were produced. Talc has typical infrared peaks at 668 and 3677 cm^{-1} (Liu et al., 2014). (c) In experiments at 300°C and 3.0 kbar with olivine and 20 wt% silica, talc was the main secondary mineral. (d) An increase in the percentage of silica (⩾40 wt%) is associated with the replacement of olivine by talc.

3.2 Quantification of serpentine and talc

Fourier-transformed infrared spectroscopy has been widely used to determine the proportions of hydrous minerals in soil samples and serpentinized peridotites, with a very low detection limit of 0.01 wt% (e.g., Foresti et al., 2003; Huang et al., 2017). Serpentine, a major hydrous mineral in olivine-experiments, was quantified using the calibration curve based on mixtures of olivine and serpentine (Huang et al., 2017). Talc is the main hydrous mineral in experiments with well-homogenized mixtures of olivine and 20–40 wt% silica. In order to determine the proportions of talc in these experiments, we prepared mixtures of olivine and talc with the percentage of talc ranging from 0 wt% to 100 wt%. Figure 5 shows that the amounts of talc are positively correlated with integrated intensity ratios $\log(A_{671}/A_{503})$ (R^2=0.98), where A_{671} is the integrated intensity of the infrared band at 671 cm^{-1} for talc due to the stretching vibration of Si-O-Mg, and A_{503} is the integrated intensity of the infrared band at 503 cm^{-1} for olivine due to the bending vibration of Si-O. Serpentine and talc are the main hydrous minerals in experiments with olivine and 10 wt% silica. The percentage of serpentine and talc in the run products was calibrated according to standard curves based on mixtures of serpentine, talc, and olivine, and the proportion of talc in the mixtures ranged from 12 wt% to 37 wt%. The amounts of talc and serpentine have a positive correlation with integrated intensity ratios of $\log(A_{609}+A_{670})/A_{503}$ (R^2=0.98, Figure 6), where A_{609} represents the integrated intensity of the infrared band at 609 cm^{-1} for serpentine, A_{670} is the integrated intensity of the infrared band at 671 cm^{-1} for talc, and A_{503} the integrated intensity of the infrared band at 503 cm^{-1} for olivine. Integrated intensities were obtained by Origin 8.6 following the same procedures for all samples. Repeated analyses (>3 times) show that the precision of calibration is ±4%.

The proportions of serpentine and talc in the run products were illustrated in Figure 7 and Table 1. In experiments at

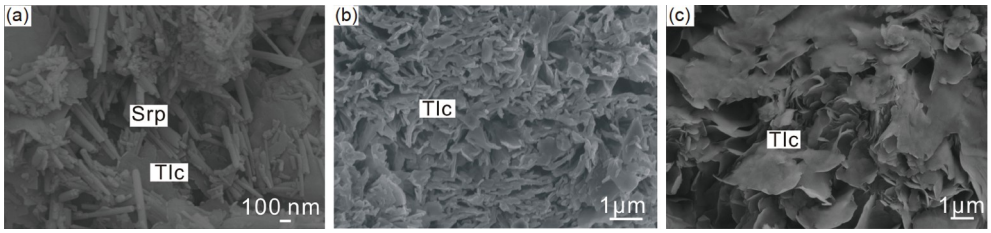

Figure 4 Scanning electron microscope images of typical run products. (a) HR116, 300°C and 3.1 kbar, mixtures of olivine and 10 wt% silica powders. Talc and fibrous chrysotile were produced. (b) HR112, 300°C and 3.1 kbar, with mixtures of olivine and 20 wt% silica. The main secondary hydrous mineral was talc. (c) HR103, 500°C and 3.0 kbar, with mixtures of olivine and 50 wt% silica. Talc with large grain sizes was formed. Tlc: talc; Srp: serpentine.

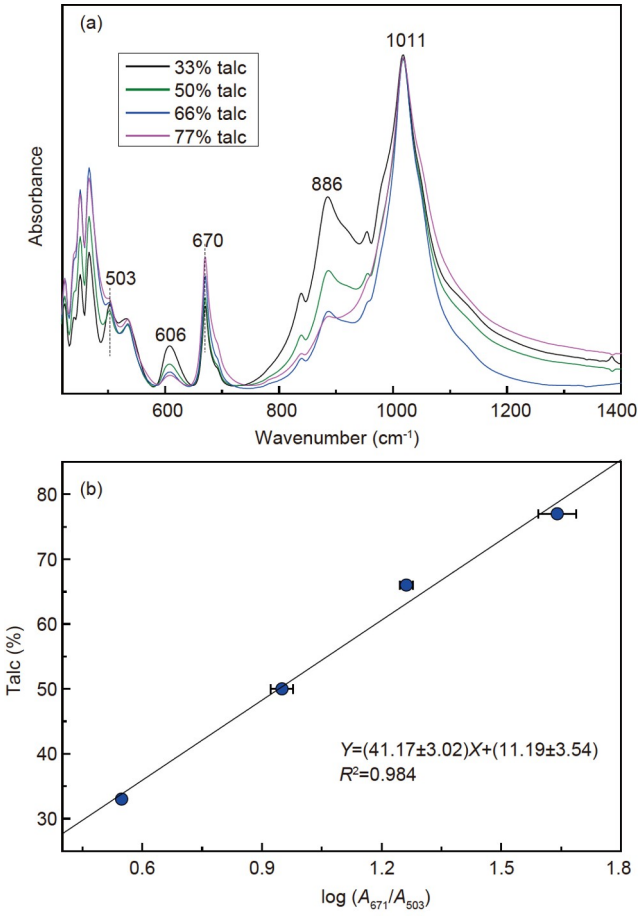

Figure 5 The standard curve for the quantification of talc in experiments with talc as the main secondary mineral. (a) Infrared spectra of well-mixed olivine and talc. With higher proportions of talc, the intensity of the infrared band at 670 cm^{-1} increases. The infrared peak at 503 cm^{-1} represents O-Mg-O band in olivine, and its intensity decreases with higher proportions of talc. (b) The standard curve used to quantify the percentage of talc in the run products. The amounts of talc are positively correlated with integrated intensity ratios $\log(A_{671}/A_{503})$ (R^2=0.98).

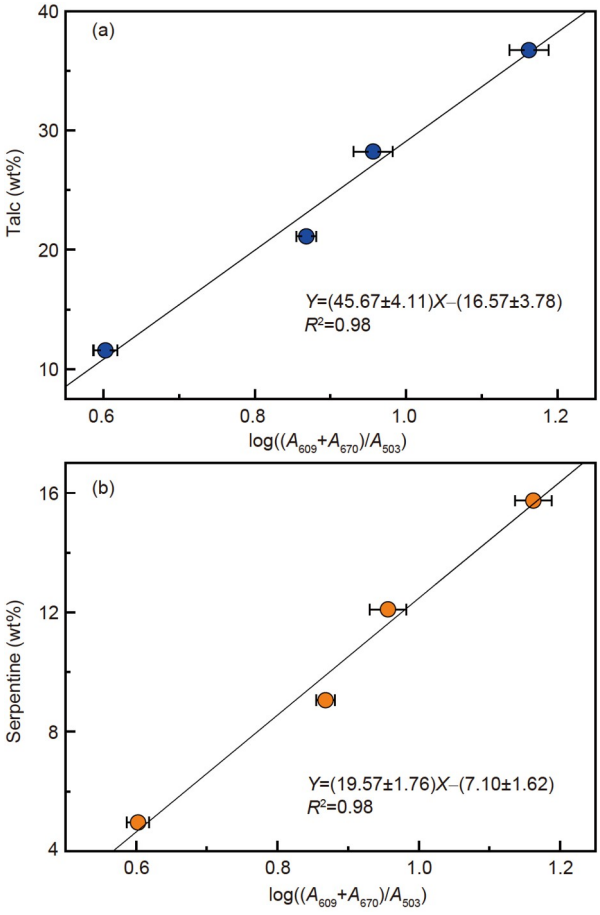

Figure 6 Standard curves for calibrating the amounts of serpentine and talc in the run products. These curves were used for experiments with serpentine and talc as main secondary minerals. (a) The standard curve for the quantification of talc. The amounts of talc are positively correlated with the integrated intensity ratios $\log(A_{609}+A_{670})/A_{503}$) ($R^2$=0.98). (b) The standard curve for the quantification of serpentine. The proportions of serpentine are positively correlated with the integrated intensity ratios $\log(A_{609}+A_{670})/A_{503}$) ($R^2$=0.98).

300°C and 3.0 kbar using well-homogenized mixtures of olivine and 10 wt% silica, the run products were composed of 10% talc and 5.5% serpentine after 7 days. The percentage of serpentine and talc was essentially unchangeable after a longer reaction period (14 days, Table 1). The overall reaction can be written as

$$4.5Mg_2SiO_4+5.5SiO_{2,aq}+4H_2O= \underset{\text{Forsterite}}{} \underset{\text{Serpentine}}{Mg_3Si_2O_5(OH)_4}+2\underset{\text{Talc}}{Mg_3Si_4O_{10}(OH)_2}. \quad (1)$$

With the addition of 20 wt% silica, the percentage of talc in

the run products was 43% after 14 days, which had no obvious increase after a longer reaction period (20 days). With the addition of 40 wt% silica, olivine was completely transformed into talc after 20 days (Figure 5). The reaction can be written as

$$\underset{\text{Forsterite}}{3Mg_2SiO_4}+5SiO_{2,aq}+2H_2O=\underset{\text{Talc}}{2Mg_3Si_4O_{10}(OH)_2}. \quad (2)$$

All these suggest that silica greatly influences reaction pathways during hydrothermal alteration of olivine. Compared to olivine-only experiments with 62% serpentine after 10 days and 76% serpentine after 27 days, the addition of 40 wt% silica promotes the hydrothermal alteration of olivine.

In olivine-experiments at 400–500°C and 3.0 kbar, the run products contained a very low percentage of serpentine (<1%) and olivine remained unaltered. Previous studies suggest that Gibbs free energies of olivine serpentinization at temperatures of ⩾350°C are positive (Allen and Seyfried, 2003; McCollom and Bach, 2009). Olivine was extensively hydrothermally altered in the presence of silica. In particular, olivine was completely transformed into talc in experiments at 505°C and 3.0 kbar with mixtures of olivine and 50 wt% silica (Figure 2; Table 1). All these suggest that silica greatly enhances the hydrothermal alteration of olivine.

3.3 Kinetics

The kinetic behavior of olivine hydrothermal alteration in this study was described by the kinetic pseudo-second-order model, which has been taken to illustrate the serpentinization of olivine and peridotite in previous studies (e.g., Lafay et al., 2012, 2014; Huang et al., 2017). The model describes the kinetics of olivine hydrothermal alteration by using the variation of alteration extent ξ(%) with time t (day). Alteration extent is defined as the proportion of secondary minerals. The differential form of the kinetic model is described as

$$\frac{d\xi}{dt}=k\left(\xi_{max}-\xi\right)^2, \quad (3)$$

where k is the rate constant, ξ_{max} is the maximum alteration extent at apparent equilibrium (%) and ξ is the alteration extent (%) at time t (day). The integral form of eq. (3) with the boundary condition t=0 and ξ=0 yields eq. (4):

$$\xi=\frac{\xi_{max}\times t}{t_{1/2}+t}, \quad (4)$$

where $t_{1/2}$ is defined as $1/(k\,\xi_{max})$, which represents the time for half of the maximum of alteration extent. The initial-rate is $v_0=\xi_{max}/t_{1/2}$.

Table 2 illustrates the kinetic parameters during olivine hydrothermal alteration. For experiments with well-mixed olivine and 10 wt% silica, the initial-rate of olivine hydrothermal alteration is 2.13×10^{-7} s^{-1}, which increased to 5.19×10^{-7} s^{-1} for experiments with 20 wt% silica, and to 4.82×10^{-6} s^{-1} for experiments with higher amounts of silica (40 wt%). This suggests that silica greatly enhances the hydrothermal alteration of olivine.

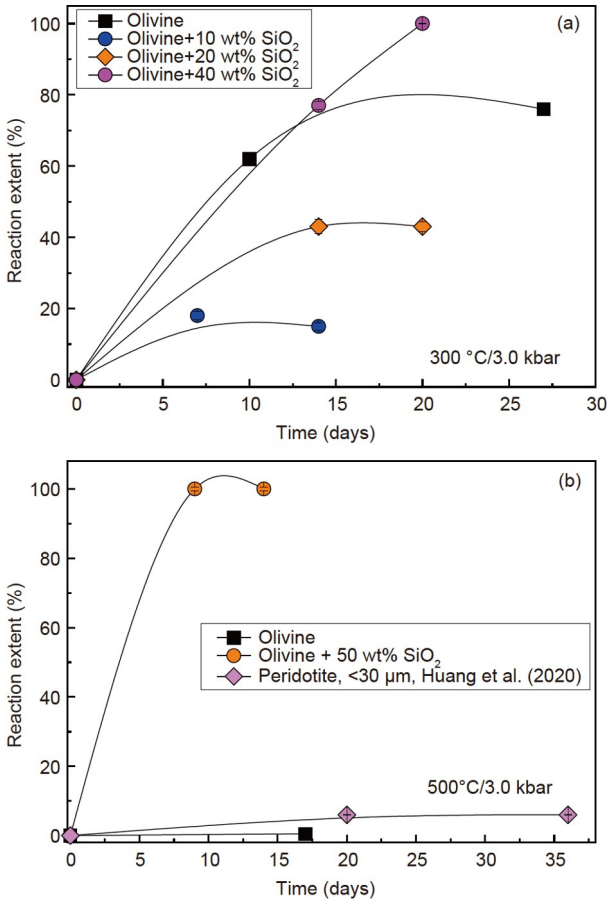

Figure 7 The extent of reaction (i.e., the proportions of secondary hydrous minerals) as a function of reaction period. The hydrous minerals of each line denote the total amounts of secondary hydrous minerals in the run products.

3.4 Molecular hydrogen (H_2) formation

Blank experiments were performed at 300–500°C and 3.0 kbar by loading olivine and SiO_2 powders into gold capsules without saline solutions. Molecular hydrogen (H_2) was below the detection limit of the gas chromatograph, which suggests that the detected H_2 is formed after the hydration of olivine rather than released from cracks and fluid inclusions of olivine. Otherwise, more concentrated dissolved H_2 would be detected.

When olivine was reacted with saline solutions at 300°C and 3.0 kbar, H_2 concentrations in fluids increased from zero to 94 mmol kg^{-1} after an experimental duration of 10 days, which decreased slightly to 80 mmol kg^{-1} after a longer period (27 days) (Table 1; Figure 8). Molecular hydrogen formation is closely associated with the oxidation of ferrous iron (Fe^{2+}) into ferric iron (Fe^{3+}). The lack of XRD peaks for magnetite indicates the formation of Fe^{3+}-bearing serpentine (Andreani et al., 2013; McCollom et al., 2016). With the

Table 2 Kinetic parameters obtained from the pseudo-second-order model

Starting materials	Temperature (°C)	ξ_{max}(%)		$t_{1/2}$ (days)	Initial rate (1 s^{-1})	Fitting r^2
		Exp.	Calc.			
Olivine	300	76	100	6.8±0.77	$1.69\times10^{-6}\pm1.92\times10^{-7}$	0.993
Olivine+10 wt% silica	300	12	100	54.2±9.5	$2.13\times10^{-7}\pm3.74\times10^{-8}$	0.890
Olivine+20 wt% silica	300	43	100	22.3±2.8	$5.19\times10^{-7}\pm6.52\times10^{-8}$	0.969
Olivine+40 wt% silica	300	100	100	2.4±1.5	$4.82\times10^{-6}\pm3.01\times10^{-5}$	0.966

addition of silica, H_2 concentrations in fluids decreased significantly. For experiments with olivine and 10% silica powders, H_2 concentrations were 8 mmol kg^{-1} after 20 days, around one order of magnitude lower compared to H_2 produced in olivine-experiments (Figure 8). With increasing amounts of silica (20 wt% and 40 wt%), a further decrease in H_2 concentrations was observed, suggesting that silica impedes molecular hydrogen (H_2) production during the hydrothermal alteration of olivine. In experiments at 400–500°C and 3.0 kbar, H_2 produced in experiments with mixtures of olivine and silica powders is essentially the same as H_2 formed in olivine-only experiments (Table 1). This suggests that the influence of silica on H_2 production during the hydrothermal alteration of olivine at 400–500°C and 3.0 kbar is negligible.

Oxygen fugacity of all the experiments in this study was quantified according to eq. (5):

$$\log f\,O_2 = 2\times\left(-\log a_{H_2} - \log K_2 - \log K_3\right), \quad (5)$$

where a_{H_2} is dissolved H_2 concentration, and K_2 and K_3 are equilibrium constants of reactions (6) and (7), respectively.

$$H_{2,aq} = H_{2,g}, \quad (6)$$

$$H_{2,g} + 0.5O_{2,g} = H_2O_1. \quad (7)$$

The activity coefficient for dissolved H_2 under the *T*-*P* conditions of this study is 1.5 (Allen and Seyfried, 2003). Equilibrium constants K_2 and K_3 were calibrated using thermodynamic data from SUPCRT 92 (Johnson et al., 1992). Figure 8b shows that oxygen fugacities in olivine-only experiments at 300°C and 3.0 kbar are very low, around four log units below the oxygen fugacity of FMQ (Fayalite-magnetite-quartz buffer assemblage), i.e., ΔFMQ-4.0. With the addition of silica powders, oxygen fugacities increase greatly, up to 0.96 log units below FMQ (ΔFMQ-0.96). This suggests that silica strongly influences the redox conditions during the hydrothermal alteration of olivine.

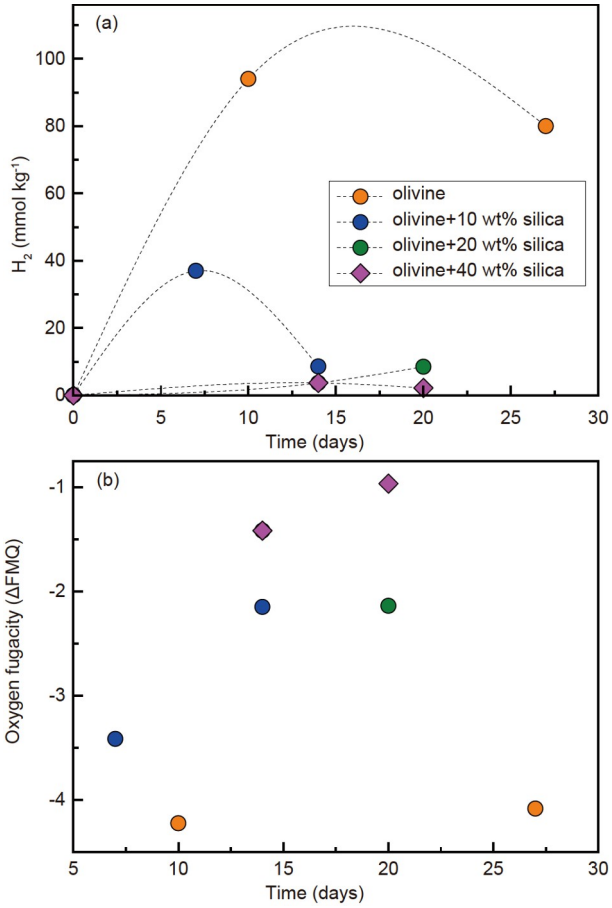

Figure 8 (a) Silica impedes greatly hydrogen formation during olivine hydrothermal alteration at 300°C and 3.0 kbar. (b) Silica increases oxygen fugacities associated with olivine hydrothermal alteration at 300°C and 3.0 kbar.

4. Discussion

4.1 Influence of silica on the thermodynamics and kinetics of olivine hydrothermal alteration

Previous experiments on olivine hydrothermal alteration have been performed mostly with pure H_2O and saline solutions (0.5 mol L^{-1} NaCl) (e.g., Martin and Fyfe, 1970; Wegner and Ernst, 1983; Marcaillou et al., 2011; Malvoisin et al., 2012; McCollom et al., 2016; Huang et al., 2017). A few experiments have been carried out at 250°C and water-vapor saturated pressures (39.8 bar) using olivine powder (140 mg, 35 mm in length) in contact with quartz powder (40 mg, 10 mm in length) (Oyanagi et al., 2015, 2020). Silica activity in one sample is largely scattered by up to four orders of magnitude, resulting in a great influence on the mineralogy of the run products. Experiments of Oyanagi et al. (2015) were performed with highly alkaline solutions

($NaOH_{aq}$, pH=13.8 at 25°C). Silica activity is highest at the olivine-quartz boundary, where smectite and serpentine are the main secondary hydrous minerals; silica activity decreases gradually away from the olivine-quartz boundary, with serpentine and brucite as the main secondary hydrous minerals (Oyanagi et al., 2015). The proportions of smectite, serpentine and brucite in the run products were determined based on analyses of SEM images, and the area proportion of smectite and serpentine close to the olivine-quartz boundary is higher than the amounts of brucite and serpentine (Oyanagi et al., 2015), suggesting that silica enhances the hydrothermal alteration of olivine. Experiments of Oyanagi et al. (2020) were performed using a similar approach to that described in Oyanagi et al. (2015), and saline solutions (0.5 mol L^{-1} NaCl) were used instead of highly alkaline solutions. With decreasing silica activity from the olivine-quartz boundary, three alteration zones were formed: talc; serpentine+talc; and serpentine+brucite+magnetite, and intermediate silica activity in the serpentine+talc zone is associated with the fastest rates of reaction (Oyanagi et al., 2020).

When silica powders were added, silica activity during the hydrothermal alteration of olivine was buffered by the reaction Quartz=$SiO_{2,aq}$. At 300°C and 3.0 kbar, silica activity ($\log aSiO_{2,aq}$) is −1.75 (Manning, 1994), which suggests that the addition of silica leads to the formation of SiO_2-bearing fluids. The reaction of olivine with SiO_2-bearing solutions produces talc and (±) serpentine, and the mineralogy of run products is greatly influenced by silica activity (Oyanagi et al., 2015, 2020). Silica in hydrothermal solutions is mainly in the complex form of H_4SiO_4, and the diffusion coefficient of H_4SiO_4 is around 1×10^{-6} cm^2 s^{-1} (Lichtner et al., 1986). The characteristic diffusion distance of H_4SiO_4 is 4.2 mm after half a day, which is much less compared to the length of olivine powders in previous experiments (35 mm), resulting in largely scattered silica activity for each sample, i.e., silica activity is highest at the olivine-quartz boundary, and it decreases gradually away from the boundary (Oyanagi et al., 2015, 2020). In particular, silica activity in one position varied with the progress of reaction, as indicated by the transformation of serpentine into talc and smectite and the migration of brucite appearance front (Oyanagi et al., 2015, 2020).

Experiments of this study were carried out with well-mixed olivine and (±) silica powders with a thickness of <2 mm. Silica activity in the experiments of this study is much less scattered compared to that in previous experiments (Oyanagi et al., 2015, 2020), as indicated by the same mineral assemblages in the run products with increasing reaction time. The experiments of this study suggest that silica greatly influences reaction pathways during olivine hydrothermal alteration, and higher silica activity is associated with a faster rate of reaction. In experiments at 300°C and 3.0 kbar with 10 wt% silica, olivine was transformed into serpentine and talc according to reaction (1) at a very slow rate, with an initial-rate of 2.13×10^{-7} s^{-1}. With increasing amounts of silica in the starting reactants (20 wt% and 40 wt%), olivine has a faster rate of hydrothermal alteration, and the initial-rate increases by around one order of magnitude. The absence of XRD peaks for silica powders in the run products suggests that olivine hydrothermal alteration proceeded under silica-understatured conditions. In contrast, relic silica powders were still observed in previous experiments (Oyanagi et al., 2015, 2020).

Previous experimental studies and thermodynamic simulations have revealed that the rates of olivine serpentinization at temperatures of ⩾350°C are very sluggish, due to positive Gibbs free energies of olivine hydrothermal alteration (Allen and Seyfried, 2003; McCollom and Bach, 2009):

$$2Mg_2SiO_4+3H_2O=Mg_3Si_2O_5(OH)_4+Mg(OH)_2. \quad (8)$$
Forsterite Serpentine Brucite

Consistently, our experiments with olivine as the solid reactant also show a very low degree of serpentine in the run products, <1%, which is associated with very low production of H_2 (Table 1). In contrast, olivine was completely transformed into talc in experiments at 500°C and 3.0 kbar with well-mixed olivine and 50 wt% silica, which indicates that the hydrothermal alteration of olivine in silica-bearing fluids is thermodynamically feasible under these *T*-*P* conditions. In order to test such a hypothesis, we calibrated Gibbs free energies of olivine hydrothermal alteration at 100–500°C and 3.0 kbar using a customized thermodynamic database compiled with SUPCRT92 (Johnson et al., 1992). Without the addition of silica, Gibbs free energies of olivine hydrothermal alteration at 400–500°C and 3.0 kbar are positive (Figure 9), which agrees well with previous studies (Allen and Seyfried, 2003; McCollom and Bach, 2009). Silica greatly decreases Gibbs free energies of olivine hydrothermal alteration that are negative at 400–500°C and 3.0 kbar (Figure 9), leading to an increase in the rates of olivine hydrothermal alteration.

Previous experiments on the serpentinization of peridotite show that pyroxene released some of its silica, and the consumption of silica by olivine hydrothermal alteration produced serpentine (Huang et al., 2020):

$$3Mg_2SiO_4+SiO_{2,aq}+4H_2O=2Mg_3Si_2O_5(OH)_4. \quad (9)$$
Forsterite Serpentine

As a result, the hydrothermal alteration of olivine was slightly enhanced, e.g., at 500°C and 3.0 kbar, ~2–7% of olivine was hydrothermally altered to form serpentine after 30 days (Huang et al., 2020). As suggested by experiments of this study, olivine can be completely transformed into talc under silica-saturated conditions (reaction (2)), suggesting that silica may be a rate-limiting factor for the hydrothermal

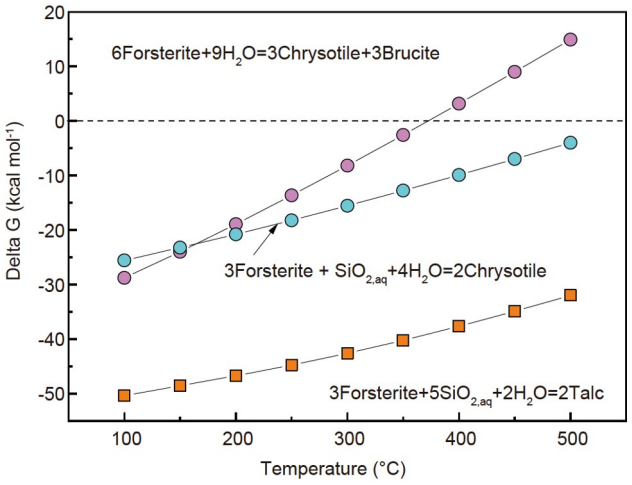

Figure 9 Effect of silica on Gibbs free energies of olivine hydrothermal alteration at 100–500°C and 3.0 kbar. Without silica, hydrothermal alteration of olivine proceeds via 6Forsterite+9H_2O=3Chrysotile+3Brucite, and Gibbs free energies at 400–500°C and 3.0 kbar are positive. With pyroxene as the source of silica, olivine hydrothermal alteration proceeds via reaction (9), and Gibbs free energies at 400–500°C and 3.0 kbar become negative. With increasing amounts of silica, the overall reaction for olivine hydrothermal alteration is reaction (2), and Gibbs free energies decrease significantly.

alteration of olivine at ⩾350°C. Interestingly, the Gibbs free energy of olivine hydrothermal alteration via reaction (2) is much lower compared to that of reaction (9) (Figure 9), which indicates that the hydrothermal alteration of olivine in SiO_2-bearing solutions at ⩾350°C is thermodynamically controlled.

4.2 Influence of silica on hydrogen formation during olivine hydrothermal alteration

The experiments of this study suggest that silica strongly inhibits hydrogen formation during olivine hydrothermal alteration at 300°C and 3.0 kbar. Hydrogen production is very high in olivine-experiments, and H_2 concentrations decreased by around two orders of magnitude in experiments with olivine and silica powders. Consistently, previous experiments also suggest a decrease in hydrogen formation during olivine hydrothermal alteration in the presence of silica-bearing minerals such as pyroxene and talc (Syverson et al., 2017; Huang et al., 2021). Pyroxene could leach silica, aluminum (Al), and chromium (Cr) during hydrothermal alteration, which greatly influence the serpentinization of olivine (Huang et al., 2020). Aluminum and Cr promote the serpentinization of olivine and enhance hydrogen production (Huang et al., 2017, 2019). Pyroxene increases the rate of olivine serpentinization (Ogasawara et al., 2013; Huang et al., 2017). However, pyroxene inhibits hydrogen formation during olivine hydrothermal alteration by around two orders of magnitude (Huang et al., 2021). Experiments of this study suggest that the negative effect of pyroxene on hydrogen formation is mainly due to the release of silica. With increasing temperatures (400–500°C and 3.0 kbar), the effect of silica on hydrogen formation during the hydrothermal alteration of olivine is negligible, and H_2 produced in experiments with well-mixed olivine and silica was essentially the same as that in olivine-experiments.

4.3 Geological implications

Silica is an important component of geological fluids. The infiltration of SiO_2-rich fluids during hydrothermal alteration of peridotite is indicated by the occurrence of talc veins in serpentinized peridotites in the Mid-Atlantic Ridge (Escartín et al., 2003; Bach et al., 2004). A decrease in MgO/SiO_2 ratios of serpentinized peridotites is proposed to result from serpentinization in SiO_2-rich fluids (Malvoisin, 2015). Serpentinites metasomatized by SiO_2-rich aqueous fluids have been reported, where serpentinites have high SiO_2 contents and orthopyroxene is hydrated to form talc and amphibole (Paulick et al., 2006; Whattam et al., 2022).

The experiments of this study were carried out using well-mixed olivine and silica powders, in great contrast with Oyanagi et al. (2015, 2020) with a high silica gradient. Our experiments suggest that silica greatly influences the reaction pathways and the rates of reaction during olivine hydrothermal alteration. The hydrothermal alteration of olivine in SiO_2-bearing fluids produces talc and (±) serpentine, and such mineral assemblage was also observed in serpentinized peridotites in the Mid-Atlantic Ridge (Escartín et al., 2003; Bach et al., 2004). When olivine is replaced by talc and serpentine, the rates of reaction are very sluggish, much slower compared to the rates of reaction in experiments with solely serpentine. At higher silica activity, olivine is replaced by talc, and the rates of reaction are much faster. In experiments at 300°C and 3.0 kbar, the hydrothermal alteration of olivine is proceeded according to reaction (1) and (2), which indicates that the reaction may be limited by silica supply. After silica powders were completely consumed, the hydrothermal alteration of olivine may be greatly influenced by talc dissolution (reaction (10)):

$$\underset{\text{Talc}}{Mg_3Si_4O_{10}(OH)_2}+H_2O=\underset{\text{Serpentine}}{Mg_3Si_2O_5(OH)_4}+2SiO_2. \quad (10)$$

In contrast, the experiments of Oyanagi et al. (2015, 2020) were performed with a high silica gradient, and olivine hydrothermal alteration is greatly influenced by the mass transport of silica. Relic silica was always observed after experiments (Oyanagi et al., 2015, 2020), which indicates that silica-saturated conditions were reached during olivine hydrothermal alteration.

The experiments of this study suggest that the infiltration of SiO_2-rich fluids during hydrothermal alteration of peridotite decreases H_2 formation. Consistently, previous ex-

periments at 300°C and 3.0 kbar suggest that pyroxene minerals released some of their silica, which inhibits the formation of H_2 during olivine hydrothermal alteration (Huang et al., 2021). Silica leached from talc decreased H_2 production during the hydrothermal alteration of olivine (Syverson et al., 2017). An inverse correlation between SiO_2 concentrations and dissolved H_2 in hydrothermal vents also indicates the negative effect of silica on H_2 formation (Seyfried et al., 2011). All these indicate that silica released from minerals (e.g., pyroxene, quartz, and talc) inhibits H_2 formation.

5. Conclusions

Hydrothermal experiments were carried out at 300–515°C and 3.0 kbar using mixtures of olivine and SiO_2 powders to study the effect of silica on olivine hydrothermal alteration and H_2 production. With the addition of 10 wt% silica, olivine was hydrothermally altered to form serpentine and talc, and the hydrothermal alteration of olivine is very sluggish. With increasing amounts of silica (20 wt% and 40 wt%), olivine was completely transformed into talc, and the rates of olivine hydrothermal alteration increased greatly. Silica inhibits molecular hydrogen (H_2) formation during olivine hydrothermal alteration at 300°C and 3.0 kbar, and the concentration of dissolved H_2 in aqueous fluids decreases by around an order of magnitude with the addition of silica. At 400–500°C and 3.0 kbar, the production of H_2 in olivine-only experiments was around one order of magnitude lower than H_2 produced at 300°C and 3.0 kbar, and it was essentially unchangeable with the addition of silica. Olivine in natural geological settings is typically intimately associated with SiO_2-bearing minerals such as plagioclase and pyroxene. Consequently, olivine hydrothermal alteration and H_2 production can be greatly influenced.

Acknowledgements *This study was supported by the National Natural Science Foundation of China (Grant No. 41873069), the Strategic Priority Research Program of the Chinese Academy of Sciences (Grant Nos. XDA22050103, XDB42000000), and the Shenzhen Municipal Natural Science Foundation (Grant No. JCYJ20220530113016038).*

Conflict of interest The authors declare that they have no conflict of interest.

References

Allen D E, Seyfried Jr W E. 2003. Compositional controls on vent fluids from ultramafic-hosted hydrothermal systems at mid-ocean ridges: An experimental study at 400°C, 500 bars. Geochim Cosmochim Acta, 67: 1531–1542

Andreani M, Muñoz M, Marcaillou C, Delacour A. 2013. µXANES study of iron redox state in serpentine during oceanic serpentinization. Lithos, 178: 70–83

Bach W, Garrido C J, Paulick H, Harvey J, Rosner M. 2004. Seawater-peridotite interactions: First insights from ODP Leg 209, MAR 15°N. Geochem Geophys Geosyst, 5: Q09F26

Beard J S, Frost B R, Fryer P, McCaig A, Searle R, Ildefonse B, Zinin P, Sharma S K. 2009. Onset and progression of serpentinization and magnetite formation in olivine-rich troctolite from IODP Hole U1309D. J Petrol, 50: 387–403

Berndt M E, Allen D E, Seyfried W E Jr. 1996. Reduction of CO_2 during serpentinization of olivine at 300°C and 500 bar. Geology, 24: 351–354

Brazelton W J, Nelson B, Schrenk M O. 2012. Metagenomic evidence for H_2 oxidation and H_2 production by serpentinite-hosted subsurface microbial communities. Front Microbio, 2, http://doi.org/10.3389/fmicb.2011.00268

Brazelton W J, Schrenk M O, Kelley D S, Baross J A. 2006. Methane- and sulfur-metabolizing microbial communities dominate the Lost City hydrothermal field ecosystem. Appl Environ Microbiol, 72: 6257–6270

Charlou J L, Donval J P, Fouquet Y, Jean-Baptiste P, Holm N. 2002. Geochemistry of high H_2 and CH_4 vent fluids issuing from ultramafic rocks at the Rainbow hydrothermal field (36°14′N, MAR). Chem Geol, 191: 345–359

Charlou J L, Fouquet Y, Bougault H, Donval J P, Etoubleau J, Jean-Baptiste P, Dapoigny A, Appriou P, Rona P A. 1998. Intense CH_4 plumes generated by serpentinization of ultramafic rocks at the intersection of the 15°20′N fracture zone and the Mid-Atlantic Ridge. Geochim Cosmochim Acta, 62: 2323–2333

Chen D G, Li B X, Zhi X C. 1994. Genetic geochemistry of mantle-derived peridotite xenolith from Panshishan, Jiangsu (in Chinese). Geochimica, 23: 13–24

Escartín J, Hirth G, Evans B. 1997. Effects of serpentinization on the lithospheric strength and the style of normal faulting at slow-spreading ridges. Earth Planet Sci Lett, 151: 181–189

Escartín J, Hirth G, Evans B. 2001. Strength of slightly serpentinized peridotites: Implications for the tectonics of oceanic lithosphere. Geology, 29: 1023

Escartín J, Mével C, MacLeod C J, McCaig A M. 2003. Constraints on deformation conditions and the origin of oceanic detachments: The Mid-Atlantic Ridge core complex at 15°45′N. Geochem Geophys Geosyst, 4, http://doi.org/10.1029/2002GC000472

Evans B W, Hattori K, Baronnet A. 2013. Serpentinite: What, why, where? Elements, 9: 99–106

Foresti E, Gazzano M, Gualtieri A F, Lesci I G, Lunelli B, Pecchini G, Renna E, Roveri N. 2003. Determination of low levels of free fibres of chrysotile in contaminated soils by X-ray diffraction and FTIR spectroscopy. Anal BioAnal Chem, 376: 653–658

Frost B R, Beard J S. 2007. On silica activity and serpentinization. J Petrol, 48: 1351–1368

Guillot S, Hattori K. 2013. Serpentinites: Essential roles in geodynamics, arc volcanism, sustainable development, and the origin of life. Elements, 9: 95–98

Hodgkinson M R S, Webber A P, Roberts S, Mills R A, Connelly D P, Murton B J. 2015. Talc-dominated seafloor deposits reveal a new class of hydrothermal system. Nat Commun, 6: 10150

Huang R F, Sun W D, Ding X, Liu J Z, Peng S B. 2015. Olivine versus peridotite during serpentinization: Gas formation. Sci China Earth Sci, 58: 2165–2174

Huang R F, Ding X, Sun W D, Shang X Q. 2021. Contrasted effect of spinel and pyroxene on molecular hydrogen (H_2) production during serpentinizationof olivine. Minerals, 11: 794

Huang R F, Song M S, Ding X, Zhu S Y, Zhan W H, Sun W D. 2017. Influence of pyroxene and spinel on the kinetics of peridotite serpentinization. J Geophys Res-Solid Earth, 122: 7111–7126

Huang R F, Sun W D, Liu J Z, Ding X, Peng S B, Zhan W H. 2016. The H_2/CH_4 ratio during serpentinization cannot reliably identify biological signatures. Sci Rep, 6: 33821

Huang R F, Sun W D, Song M S, Ding X. 2019. Influence of pH on molecular hydrogen (H_2) generation and reaction rates during serpentinization of peridotite and olivine. Minerals, 9: 661

Huang R, Sun W D, Ding X, Zhao Y S, Song M S. 2020. Effect of pressure on the kinetics of peridotite serpentinization. Phys Chem Miner, 47: 33

Jeanloz R. 1980. Infrared spectra of olivine polymorphs: α, β phase and spinel. Phys Chem Miner, 5: 327–341
Johnson J W, Oelkers E H, Helgeson H C. 1992. SUPCRT92: A software package for calculating the standard molal thermodynamic properties of minerals, gases, aqueous species, and reactions from 1 to 5000 bar and 0 to 1000°C. Comput Geoscis, 18: 899–947
Jöns N, Kahl W A, Bach W. 2017. Reaction-induced porosity and onset of low-temperature carbonation in abyssal peridotites: Insights from 3D high-resolution microtomography. Lithos, 268-271: 274–284
Katayama I, Kurosaki I, Hirauchi K I. 2010. Low silica activity for hydrogen generation during serpentinization: An example of natural serpentinites in the Mineoka ophiolite complex, central Japan. Earth Planet Sci Lett, 298: 199–204
Kelley D S, Karson J A, Blackman DK,Früh-Green GL, Früh-Green G L, Butterfield D A, Lilley M D, Olson E J, Schrenk M O, Roe K K, Lebon G T, Rivizzigno P. 2001. An off-axis hydrothermal vent field near the Mid-Atlantic Ridge at 30°N. Nature, 412: 145–149
Lafay R, Montes-Hernandez G, Janots E, Chiriac R, Findling N, Toche F. 2012. Mineral replacement rate of olivine by chrysotile and brucite under high alkaline conditions. J Cryst Growth, 347: 62–72
Lafay R, Montes-Hernandez G, Janots E, Chiriac R, Findling N, Toche F. 2014. Simultaneous precipitation of magnesite and lizardite from hydrothermal alteration of olivine under high-carbonate alkalinity. Chem Geol, 368: 63–75
Lang S Q, Butterfield D A, Schulte M, Kelley D S, Lilley M D. 2010. Elevated concentrations of formate, acetate and dissolved organic carbon found at the Lost City hydrothermal field. Geochim Cosmochim Acta, 74: 941–952
Lichtner P C, Oelkers E H, Helgeson H C. 1986. Interdiffusion with multiple precipitation/dissolution reactions: Transient model and the steady-state limit. Geochim Cosmochim Acta, 50: 1951–1966
Liu X W, Liu X X, Hu Y H. 2014. Investigation of the thermal decomposition of talc. Clays Clay Miner, 62: 137–144
Malvoisin B, Zhang C, Müntener O, Baumgartner L P, Kelemen P B. 2020. Measurement of volume change and mass transfer during serpentinization: Insights from the Oman Drilling Project. J Geophys Res-Solid Earth, 125: e2019JB018877
Malvoisin B, Brunet F, Carlut J, Rouméjon S, Cannat M. 2012. Serpentinization of oceanic peridotites: 2. Kinetics and processes of San Carlos olivine hydrothermal alteration. J Geophys Res, 117: B04102
Malvoisin B. 2015. Mass transfer in the oceanic lithosphere: Serpentinization is not isochemical. Earth Planet Sci Lett, 430: 75–85
Manning C E. 1994. The solubility of quartz in H_2O in the lower crust and upper mantle. Geochim Cosmochim Acta, 58: 4831–4839
Marcaillou C, Muñoz M, Vidal O, Parra T, Harfouche M. 2011. Mineralogical evidence for H_2 degassing during serpentinization at 300°C/300 bar. Earth Planet Sci Lett, 303: 281–290
Martin B, Fyfe W S. 1970. Some experimental and theoretical observations on the kinetics of hydration reactions with particular reference to serpentinization. Chem Geol, 6: 185–202
McCollom T M, Klein F, Moskowitz B, Berquó T S, Bach W, Templeton A S. 2020. Hydrogen generation and iron partitioning during experimental serpentinization of an olivine-pyroxene mixture. Geochim Cosmochim Acta, 282: 55–75
McCollom T M, Klein F, Robbins M, Moskowitz B, Berquó T S, Jöns N, Bach W, Templeton A. 2016. Temperature trends for reaction rates, hydrogen generation, and partitioning of iron during experimental serpentinization of olivine. Geochim Cosmochim Acta, 181: 175–200
McCollom T M, Bach W. 2009. Thermodynamic constraints on hydrogen generation during serpentinization of ultramafic rocks. Geochim Cosmochim Acta, 73: 856–875
Mével C. 2003. Serpentinization of abyssal peridotites at mid-ocean ridges. Comptes Rendus Geosci, 335: 825–852
Miyoshi A, Kogiso T, Ishikawa N, Mibe K. 2014. Role of silica for the progress of serpentinization reactions: Constraints from successive changes in mineralogical textures of serpentinites from Iwanaidake ultramafic body, Japan. Am Mineral, 99: 1035–1044
Ogasawara Y, Okamoto A, Hirano N, Tsuchiya N. 2013. Coupled reactions and silica diffusion during serpentinization. Geochim Cosmochim Acta, 119: 212–230
Okamoto A, Ogasawara Y, Ogawa Y, Tsuchiya N. 2011. Progress of hydration reactions in olivine-H_2O and orthopyroxenite-H_2O systems at 250°C and vapor-saturated pressure. Chem Geol, 289: 245–255
Oyanagi R, Okamoto A, Hirano N, Tsuchiya N. 2015. Competitive hydration and dehydration at olivine–quartz boundary revealed by hydrothermal experiments: Implications for silica metasomatism at the crust–mantle boundary. Earth Planet Sci Lett, 425: 44–54
Oyanagi R, Okamoto A, Tsuchiya N. 2020. Silica controls on hydration kinetics during serpentinization of olivine: Insights from hydrothermal experiments and a reactive transport model. Geochim Cosmochim Acta, 270: 21–42
Pan C C, Yu L P, Liu J Z, Fu J M. 2006. Chemical and carbon isotopic fractionations of gaseous hydrocarbons during abiogenic oxidation. Earth Planet Sci Lett, 246: 70–89
Paulick H, Bach W, Godard M, De Hoog J C M, Suhr G, Harvey J. 2006. Geochemistry of abyssal peridotites (Mid-Atlantic Ridge, 15°20′N, ODP Leg 209): Implications for fluid/rock interaction in slow spreading environments. Chem Geol, 234: 179–210
Scambelluri M, Fiebig J, Malaspina N, Müntener O, Pettke T. 2004. Serpentinite subduction: Implications for fluid processes and trace-element recycling. Int Geol Rev, 46: 595–613
Scambelluri M. 2001. Serpentinite: A trace-element study of the Erro-Tobbio high-pressure ultramafites (Western Alps, NW Italy). J Petrol, 42: 55–67
Schrenk M O, Brazelton W J, Lang S Q. 2013. Serpentinization, carbon, and deep life. Rev Mineral Geochem, 75: 575–606
Schrenk M O, Kelley D S, Bolton S A, Baross J A. 2004. Low archaeal diversity linked to subseafloor geochemical processes at the Lost City hydrothermal field, mid-Atlantic ridge. Environ Microbiol, 6: 1086–1095
Seyfried W E Jr, Pester N J, Ding K, Rough M. 2011. Vent fluid chemistry of the Rainbow hydrothermal system (36°N, MAR): Phase equilibria and *in situ* pH controls on subseafloor alteration processes. Geochim Cosmochim Acta, 75: 1574–1593
Sun W, Peng Z, Zhi X, Chen D, Wang Z, Zhou X. 1998. Osmium isotope determination on mantle-derived peridotite xenoliths from Panshishan with N-TIMS. Chin Sci Bull, 43: 573–575
Syverson D D, Tutolo B M, Borrok D M, Seyfried W E Jr. 2017. Serpentinization of olivine at 300 °C and 500 bars: An experimental study examining the role of silica on the reaction path and oxidation state of iron. Chem Geol, 475: 122–134
Ulmer P, Trommsdorff V. 1995. Serpentine stability to mantle depths and subduction-related magmatism. Science, 268: 858–861
Wegner W W, Ernst W G. 1983. Experimentally determined hydration and dehydration reaction rates in the system MgO-SiO_2-H_2O. Am J Sci, 283-A: 151–180
Whattam S A, Früh-Green G L, Cannat M, De Hoog J C M, Schwarzenbach E M, Escartin J, John B E, Leybourne M I, Williams M J, Rouméjon S, Akizawa N, Boschi C, Harris M, Wenzel K, McCaig A, Weis D, Bilenker L. 2022. Geochemistry of serpentinized and multiphase altered Atlantis Massif peridotites (IODP Expedition 357): Petrogenesis and discrimination of melt-rock vs. fluid-rock processes. Chem Geol, 594: 120681
Xiong Y, Geng A, Wang Y, Liu D, Jia R, Shen J, Xiao X. 2001. Kinetic simulating experiment on the secondary hydrocarbon generation of kerogen. Sci China Ser D-Earth Sci, 45: 13–20
Xu X S, Griffin W L, O'Reilly S Y, Pearson N J, Geng H Y, Zheng J P. 2008. Re-Os isotopes of sulfides in mantle xenoliths from eastern China: Progressive modification of lithospheric mantle. Lithos, 102: 43–64

(Editorial handling: Huaiwei NI)